The influence of central black holes on gravitational lenses

Mao, Shude; Witt, Hans J.; Koopmans, Leon V. E.

Published in:
Monthly Notices of the Royal Astronomical Society

DOI:
10.1046/j.1365-8711.2001.04143.x

Publication date:
2001

Mon. Not. R. Astron. Soc. **323**, 301–307 (2001)

The influence of central black holes on gravitational lenses

Shude Mao,[1★] Hans J. Witt[2★] and Leon V. E. Koopmans[1★]
[1]*University of Manchester, Jodrell Bank Observatory, Macclesfield, Cheshire SK11 9DL*
[2]*Astrophysikalisches Institut Potsdam, An der Sternwarte 16, 14482 Potsdam, Germany*

Accepted 2000 October 20. Received 2000 October 13; in original form 2000 July 5

ABSTRACT

Recent observations indicate that many if not all galaxies host massive central black holes. In this paper we explore the influence of black holes on the lensing properties. We model the lens as an isothermal ellipsoid with a finite core radius plus a central black hole. We show that the presence of the black hole substantially changes the critical curves and caustics. If the black hole mass is above a critical value, then it will completely suppress the central images for all source positions. Realistic central black holes are likely to have masses below this critical value. Even in such subcritical cases, the black hole can suppress the central image when the source is inside a zone of influence, which depends on the core radius and black hole mass. In the subcritical cases, an additional image may be created by the black hole in some regions, which for some radio lenses may be detectable with high-resolution and large dynamic range VLBI maps. The presence of central black holes should also be taken into account when one constrains the core radius from the lack of central images in gravitational lenses.

Key words: gravitational lensing – galaxies: nuclei – galaxies: structure – cosmology: theory – dark matter.

1 INTRODUCTION

Recent observations suggest that many if not all nearby galaxies host massive central black holes (e.g. Kormendy & Richstone 1995; Magorrian et al. 1998). The existence of such central black holes can be accommodated by hierarchical structure formation theories (e.g. Silk & Rees 1998; Kauffmann & Haehnelt 2000). The effects of central black holes on gravitational lensing have not been studied in detail, although it is commonly believed that the central singularity can suppress the central image. This is important because lensing theories predict that any *non-singular* lens should have an odd number of images, while the observed lenses always show an even number of images (Burke 1981; see also Schneider, Ehlers & Falco 1992 for a general review on gravitational lensing); the only possible exception is APM 08279+5255 (Ibata et al. 2000). The lack of central images could indicate either that the potential is singular or that the central surface density in lenses is so high that the central image is highly demagnified and thus unobservable in current surveys (Narayan, Blandford & Nityananda 1984). The purpose of this paper is to clarify, through simple examples, the effects of central black holes on lensing properties. We show that the presence of black holes can not only suppress but also create additional images. These additional images may be observable in some cases. Central black holes also introduce somewhat unusual critical curves and caustic structures. The outline of this paper is as follows. In Section 2, we first outline the lensing basics and derive some analytical results for the critical curves, caustics and image properties for an isothermal sphere plus a black hole. We then generalize to the case of an isothermal ellipsoid plus a black hole. In Section 3, we discuss the implications of black holes on gravitational lenses, including the constraints on the core radius.

★ E-mail: smao@jb.man.ac.uk (SM); hwitt@aip.de (HJW); leon@jb.man.ac.uk (LVEK)

2 EFFECTS OF CENTRAL BLACK HOLES ON LENSING

We model a lensing galaxy as an isothermal ellipsoid plus a central black hole. The isothermal ellipsoid model is not only analytically tractable but also consistent with models of individual lenses, lens statistics, stellar dynamics and X-ray galaxies (e.g. Fabbiano 1989; Maoz & Rix 1993; Kochanek 1995, 1996b; Grogin & Narayan 1996a,b; Rix et al. 1997). The surface density distribution of an isothermal ellipsoid is given by

$$\frac{\Sigma}{\Sigma_{\rm cr}} = \frac{1}{2q}\frac{1}{\sqrt{x^2 + y^2/q^2 + r_{\rm c}^2}}, \qquad (1)$$

where $r_{\rm c}$ is the core radius, q is the axial ratio and $\Sigma_{\rm cr} = c^2 D_{\rm s}/(4\pi G D_{\rm l} D_{\rm ls})$ is the critical surface density, $D_{\rm l}$, $D_{\rm s}$ are angular diameter distances from the observer to the lens and source, respectively, and $D_{\rm ls}$ is the angular diameter distance from the lens

to the source. Note that all the lengths (x, y, r_c) are expressed in units of the critical radius, R_{cr},

$$R_{cr} = D_l b, \qquad b \equiv 4\pi\left(\frac{\sigma}{c}\right)^2 \frac{D_{ls}}{D_s}, \tag{2}$$

where the critical angle b is the angle extended by the critical radius on the sky ($b \sim 0.2$–3 arcsec for typical lens galaxies; e.g. Jackson et al. 1998), and the velocity dispersion σ in equation (2) is related to, but not identical to, the observable line-of-sight velocity dispersion; we shall ignore this minor complication in our analysis and simply treat it as a parameter (see Keeton, Kochanek & Seljak 1997 for further discussions).

The lensing properties of the isothermal ellipsoid have been given by Kassiola & Kovner (1993), Kormann, Schneider & Bartelmann (1994), and Keeton & Kochanek (1998). The lens equation of an isothermal ellipsoid plus a black hole is

$$u = x - \frac{1}{\sqrt{1-q^2}} \tan^{-1}\left(\frac{\sqrt{1-q^2}x}{\varphi + r_c}\right) - m\frac{x}{r^2},$$

$$v = y - \frac{1}{\sqrt{1-q^2}} \tanh^{-1}\left(\frac{\sqrt{1-q^2}y}{\varphi + q^2 r_c}\right) - m\frac{y}{r^2}, \tag{3}$$

where $\varphi^2 = q^2(r_c^2 + x^2) + y^2, r^2 = x^2 + y^2$, and the dimensionless black hole mass is given by

$$m = \frac{M_{bh}}{M_0}, \qquad M_0 \equiv \frac{\pi\sigma^2 R_{cr}}{G}, \tag{4}$$

with M_{bh} being the mass of the black hole. Physically, M_0 is the mass of the galaxy contained within a cylinder with radius R_{cr} and hence m_0 is essentially the ratio of the black hole mass to the mass of the galaxy in the inner parts (within R_{cr}). The magnification (μ) of a given image is given by

$$\mu^{-1} = \frac{\partial u}{\partial x}\frac{\partial v}{\partial y} - \frac{\partial v}{\partial x}\frac{\partial u}{\partial y}. \tag{5}$$

For definitiveness, we shall adopt a lens redshift of 0.5 and a source redshift of 2. In the Einstein–de Sitter universe ($\Omega_0 = 1$ with no cosmological constant), the angular and length units are given by

$$b = 1''\left(\frac{\sigma}{250}\right)^2, \qquad R_{cr} = 3.6\, h^{-1}\,\mathrm{kpc}\left(\frac{\sigma}{250}\right)^2, \tag{6}$$

where h is the Hubble constant in units of $100\,\mathrm{km\,s^{-1}\,Mpc^{-1}}$ and σ is in units of $\mathrm{km\,s^{-1}}$. The dimensionless black hole mass for the given lens and source redshifts is

$$m = 2.4 \times 10^{-3}\, h\left(\frac{\sigma}{250}\right)^{3.27}, \tag{7}$$

where we have used the tight correlation of the black hole mass with velocity dispersion found by Ferrarese & Merritt (2000), $M_{bh} \approx 4 \times 10^8\,\mathrm{M_\odot}(\sigma/250)^{5.27}$ (see Gebhardt et al. 2000 for a different scaling).[1]

The lens equation (equation 3) can be readily solved numerically. In general there are several curves in the image plane along which the magnification is infinite ($\mu^{-1} = 0$). These are called 'critical curves', and they map to 'caustics' in the source plane. Caustics mark discontinuities in the number of images, so in order to determine the number of images produced by a lens model, it is sufficient to examine the caustics. We shall consistently employ this idea in this paper. In order to gain some analytical insights into the influence of central black holes, we start with the spherical case (i.e. $q = 1$) in the next subsection.

[1] We neglect any possible evolution of the black hole mass with time.

2.1 Spherical isothermal models with black holes

For the spherical case ($q = 1$), the surface density is given by

$$\frac{\Sigma}{\Sigma_{cr}} = \frac{1}{2\sqrt{r^2 + r_c^2}}. \tag{8}$$

This profile has been studied quite extensively by Hinshaw & Krauss (1987).

The lens equation for this profile in the presence of a black hole is quite simple,

$$r_s = r - \alpha(r), \qquad \alpha(r) = \frac{\sqrt{r^2 + r_c^2} - r_c}{r} + \frac{m}{r}, \tag{9}$$

where r_s and r_c are the source position and core radius in units of the critical radius and m is the dimensionless mass of the central black hole given in equation (4).

2.1.1 Critical curves and caustics

The critical curves are given by the equation

$$\mu^{-1} = \frac{r_s}{r}\frac{\mathrm{d}r_s}{\mathrm{d}r} = 0. \tag{10}$$

The solution satisfies either $r_s/r = 0$ or $\mathrm{d}r_s/\mathrm{d}r = 0$. One can verify that the first condition ($r_s/r = 0$) always yields one single critical curve,

$$r^2 = \tfrac{1}{2}\left[1 - 2r_c + 2m + \sqrt{(1-2r_c)^2 + 4m}\right], \tag{11}$$

which maps to a degenerate caustic point at the origin. The second condition ($\mathrm{d}r_s/\mathrm{d}r = 0$) can be manipulated into a polynomial

$$\begin{aligned} r^6 + {} & (2m - 2r_c + r_c^2)r^4 \\ & + (m^2 - 2mr_c + r_c^2 + 2mr_c^2 - 2r_c^3)r^2 \\ & + m^2 r_c^2 - 2mr_c^3 = 0. \end{aligned} \tag{12}$$

This equation is cubic in r^2, and so can be solved analytically. One finds that beyond a critical black hole mass, there is no physical solution (i.e. positive solution in r^2), while below the critical mass, there are always two physical solutions. The critical mass can be found by examining equation (12); some algebra yields the critical mass

$$m_{cr} = r_c(1 + r_c) - 3\left(\frac{r_c^2}{2}\right)^{2/3}. \tag{13}$$

For a given core radius, the central images are always suppressed by the black hole if its mass exceeds the critical value, $m_{cr} \approx r_c$ when $r_c \ll 1$. This can be understood intuitively as follows: when the mass is comparable to r_c, the mass of the black hole is comparable to the galaxy mass enclosed by the core radius, so the black hole makes the deflection angle nearly flat at $r \sim r_c$, similar to the singular isothermal case, for which we have only two images (cf. Fig. 2, later). Notice, however, that even when the black hole mass is below the critical value, there is a region in the source plane where the central image is suppressed (see below).

We can obtain approximate but more illuminating solutions for

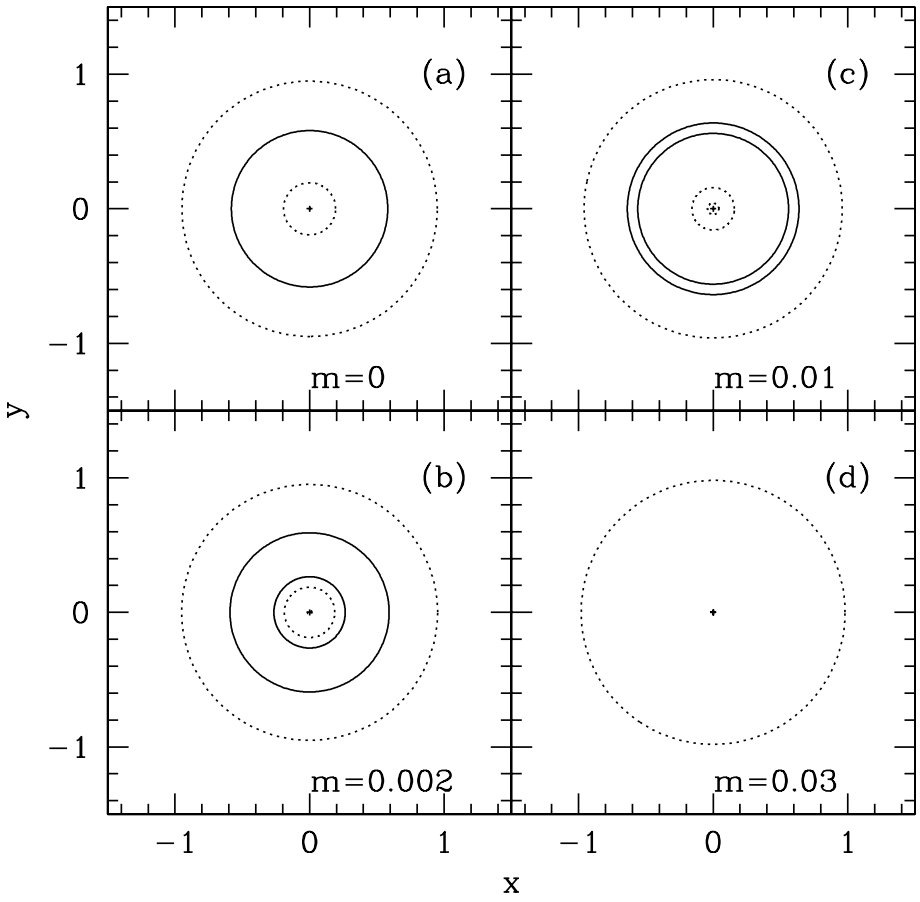

Figure 1. The critical curves (dotted) and caustics (solid) for a spherical isothermal sphere with a black hole. The core radius is $r_c = 0.05$. All the lengths are in units of the critical radius (equation 2). Each panel is labelled by the dimensionless black hole mass (m), given in equation (4), which is essentially the ratio of the black hole mass to the mass of the galaxy within the critical radius. The critical mass for this case is $m \approx 0.0175$. Note that there is a degenerate caustic point at the origin, indicated by a small plus sign. There is a tiny critical curve around the origin for $m = 0.002$, but it is too small to see clearly.

the positions of critical curves and caustics when $r_c \ll 1$ and $m \ll m_{cr} \approx r_c$. The first assumption ($r_c \ll 1$) is supported by the lack of central images in lenses (e.g. Wallington & Narayan 1993; Kochanek 1996a; see also Section 2.1.2), while the second condition is valid for most galaxies as can be seen from equation (7), and if $r_c \gtrsim 0.002$ ($\sim$10 pc for $\sigma = 250\,\mathrm{km\,s^{-1}}$). Under these two assumptions, the inner most critical curve satisfies $r \ll r_c$ (justified below), the lens equation [equation (9)] simplifies to

$$r_s = (1 - \kappa_c)r - \frac{m}{r}, \tag{14}$$

where $\kappa_c \equiv 1/(2r_c)$ is the central surface density of the galaxy, in the absence of the black hole. From this simplified lens equation, one can readily show that the innermost critical curve forms where $\mathrm{d}r_s/\mathrm{d}r = 0$, i.e.

$$r_{crit,1} = \sqrt{\frac{m}{\kappa_c - 1}}. \tag{15}$$

The second assumption (i.e. $m \ll m_{cr}$) ensures that our condition, $r \ll r_c$, is satisfied. The corresponding caustic in the source plane is

$$r_{caust,1} = -2\sqrt{m(\kappa_c - 1)} = -2mr_{crit,1}^{-1}. \tag{16}$$

The middle critical curve in general does not satisfy the condition $r \ll r_c$. To derive its approximate position, we simplify equation (12) by setting $m = 0$, after which we are left with a quadratic equation in r^2. One finds that, to the leading order of r_c, the positions of the critical curves and caustics are

$$r_{crit,2} \approx \sqrt{r_c}, \qquad r_{caust,2} \approx 1 - 2\sqrt{r_c} = 1 - 2r_{crit,2}. \tag{17}$$

From equation (11) one finds that the outermost critical curve and its corresponding caustic are at

$$r_{crit,3} \approx 1 - r_c, \qquad r_{caust,3} = 0. \tag{18}$$

For a source located outside $r_{caust,2}$ there are only two images. When a source is between $r_{caust,1}$ and $r_{caust,2}$, there are four images; compared with the case without a black hole, one additional image has been created very close to the black hole. For a source inside $r_{caust,1}$, there are only two images, the central image that would be present without a black hole has been suppressed. The radius $r_{caust,1}$ can therefore be regarded as a measure of the zone of influence of the black hole: for any source $r_s < r_{caust,1} \approx (2m/r_c)^{1/2}$, the central image is destroyed. Note that this zone of influence scales as $\propto m^{1/2}$, identical to the scaling of the Einstein radius of an isolated black hole with mass.

Fig. 1 illustrates the evolution of critical curves and caustics with the mass of the black hole increasing from zero to 0.03. The core radius is taken to be 0.05, a somewhat arbitrary value which satisfies the upper limit inferred from the lack of central images (e.g. Wallington & Narayan 1993; Kochanek 1996a). When there is no black hole at the centre (Fig. 1a) the critical curves are two

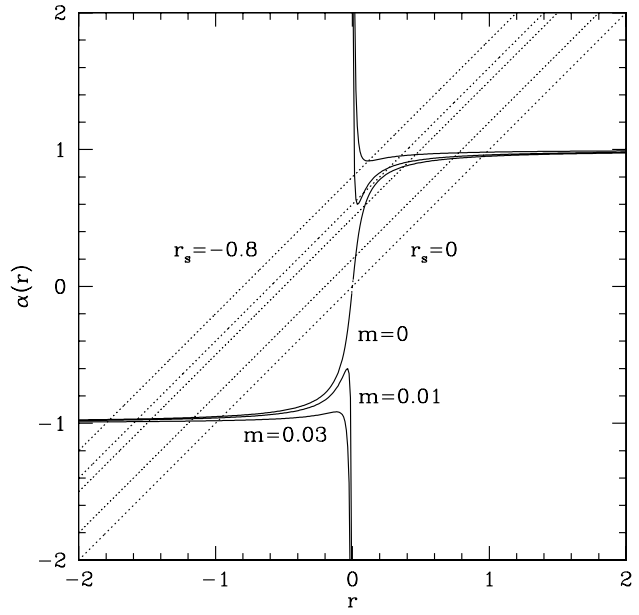

Figure 2. Deflection angle versus the radius, shown for three black hole masses, $m = 0$, 0.01 and 0.03 (from bottom to top at positive r). The parameter m is the ratio of the black hole mass to the mass of the galaxy contained within the cylinder of radius equal to the critical radius. The five dotted straight lines indicate $r_s = -0.8$, -0.6, -0.5, -0.2 and 0 (from top to bottom). For each source position, the image positions are given by the intercepts of the deflection angle curve with the straight line corresponding to the source position. Notice how the image number and position change as the source position changes.

circles, the outer critical curve maps to a degenerate caustic point at the origin, while the inner critical curve maps to the full circle. Fig. 1(b) shows the configuration when we include a black hole mass with $m = 0.002$, a value expected for a galaxy with $\sigma \approx 250\,\mathrm{km\,s^{-1}}$ [cf. equation (7)]. In addition to the two critical curves found when $m = 0$, an additional tiny critical curve appears around the origin (too small to be seen), which maps to the inner full circle. The positions of the three critical curves and their corresponding caustics are well approximated by equations (15)–(18). For a source moving from infinity to the origin, it would first have two images, and then four images as the source moves across the first caustic. Compared with the case without a black hole, one additional image has been created very close to the black hole. The number of images decreases to 2 again as the source moves across the second caustic. Note that even in this case where the black hole mass is substantially below the critical mass $m = m_{\rm cr} \approx 0.0175$, the zone of influence determined by $r_{\rm caust,1} \approx 0.28$ is substantial. Within the zone of influence, the central image is completely suppressed. When the black hole mass is further increased to $m = 0.01$ (Fig. 1c), the innermost critical curve becomes larger while the middle critical curve shrinks, their corresponding caustics also approach each other. When the black hole mass is increased to the critical mass $m_{\rm cr}$ (equation 13), the two critical curves merge into a single curve, so do their corresponding caustics. When the black hole mass is increased above the critical value (an example is shown for $m = 0.03$ in Fig. 1d), one is left with a single critical curve and a degenerate caustic point at the centre. In this case, there are only two images no matter where the source is. Notice, however, that the black hole mass for Figs 1(c) and (d) are somewhat unrealistic (cf. equation 7).

The change of image numbers may appear puzzling at first, but can be easily understood in the conventional diagram of the deflection angle, $\alpha(r)$, versus radius, shown in Fig. 2. Three examples are shown for $r_c = 0.05$ corresponding to three black hole masses, $m = 0$, 0.01 and 0.03. For each source position, the image positions are given by the intercepts of the deflection angle curve with the straight line $f(r) = r - r_s$. For example, it is easy to see why for $m = 0.01$, there are three critical curves. It is clear from this figure that the central black hole does not perturb the two outer images very much, as expected, it only strongly perturbs the central images.

2.1.2 *Image positions and magnifications*

In this subsection, we will obtain approximate image positions and magnifications when there are four images, i.e. when the source position is between $r_{\rm caust,1}$ and $r_{\rm caust,2}$. We are particularly interested in the case when the source is close to $r_{\rm caust,1}$. For such cases, there are usually two bright outer images and two faint central images; one of the fainter central images is created by the black hole. We would like to address the question of whether such images are observable.

Using the resultant technique as discussed in Witt & Mao (1995), one can verify that the four image magnifications must satisfy an exact relation

$$\mu_1 + \mu_2 + \mu_3 + \mu_4 = 2. \tag{19}$$

Note that all the magnifications include their parities (signs).

The brightest image has positive parity and is located in regions where $r \gg r_c$. For this image, the lens equation can be simplified into $r^2 - r_s r + r_c - r = 0$, where we have only retained terms to the order of $(r_c/r)^2$. From this equation, we can obtain the position and magnification of the brightest image

$$r_1 \approx 1 + r_s - r_c \quad \text{and} \quad \mu_1^{-1} \approx \frac{r_s}{r_1^3}(r_1^2 + m - r_c) \approx \frac{r_s}{r_1}. \tag{20}$$

Similarly, we can obtain the position for the bright outer image that has negative parity

$$r_2 \approx -1 + r_s + r_c \quad \text{and} \quad \mu_2^{-1} \approx \frac{r_s}{r_2}. \tag{21}$$

For singular isothermal spheres ($r_c = 0$), the magnifications and positions are exact for these two images, and they satisfy $\mu_1 + \mu_2 = 2$.

For the two central images, we can estimate their positions and magnifications if they satisfy $r \ll r_c$. In this case, the lens equation can be approximated by equation (14) and the image magnification is given by

$$\mu = \frac{1}{(1-\kappa_c)^2 - m^2/r^4}. \tag{22}$$

For very small m we can obtain for the positions and magnifications for the third and fourth image,

$$r_3 \approx -\frac{r_s}{\kappa_c - 1} \quad \text{and} \quad \mu_3 \approx \mu_c, \quad \mu_c \equiv \frac{1}{(\kappa_c - 1)^2} \tag{23}$$

$$r_4 \approx -\frac{m}{r_s} \quad \text{and} \quad \mu_4^{-1} \approx -\frac{r_s}{r_4^3}(r_s r_4 + 2m) = -\frac{r_s^4}{m^2}. \tag{24}$$

Note that the magnification for the third image $\mu_3 \sim \kappa_c^{-2} = 4r_c^2$, is independent of the source position when the black hole mass is small. Previous studies neglected the role of central black holes

and therefore the lack of central images immediately implies an upper limit on the core radius. If the brightest image is magnified by a factor of a few, and no central image is seen with a dynamic range of 100, then this would imply $r_c \lesssim 0.1$, which is roughly the published upper limits on the core radius from lenses (e.g. Wallington & Narayan 1993; Kochanek 1996a). Hence the lack of central images in lenses may mean either that the core radius is small (see Section 2.1.2) or that the black hole mass is quite massive; we return to this point in the discussion.

The fourth central image is usually the closest to the black hole and is usually very faint. However, when the source lies very close to $r_{\rm caust,1}$, the second term in the denominator of equation (22), which is the square of the shear ($\gamma_{\rm BH}$) from the black hole, can become comparable to $(1-\kappa_c)$, and then the magnification is of the order of unity or higher. The question is: how large is this region? To estimate this, we combine equations (15) and (22) and find that the position of the image is related to its magnification by

$$\left(\frac{r}{r_{\rm crit,1}}\right)^4 = \left(1-\frac{\mu_c}{\mu}\right)^{-1}, \tag{25}$$

where μ_c is the magnification of an image formed well within the core radius in the absence of the black hole and is given in equation (23). A small displacement Δr from the critical curve is related to the magnification through

$$\Delta r = \frac{\mu_c}{4\mu} r_{\rm crit,1}. \tag{26}$$

This displacement is related to a corresponding displacement of the source in the source plane, through equation (14). By definition the first-order term of a Taylor expansion of the lens equation vanishes near the caustic. The second term, after some algebra, gives

$$\Delta r_s = -\frac{m}{r_{\rm crit,1}^3}\Delta r^2 = -\frac{\sqrt{m}\mu_c^{7/4}}{16\mu^2}. \tag{27}$$

The probability of the source in a multiply imaged system, lying inside this region (i.e. having a magnification $>\mu$), is therefore

$$P_{\rm BH}(>\mu) = \frac{2r_{\rm caust,1}\Delta r_s}{r_{\rm caust,2}^2} = \frac{m\mu_c^{3/2}}{4\mu^2(1-2\sqrt{r_c})^2}. \tag{28}$$

For any realistic situation, this probability is exceedingly small ($\ll 10^{-6}$); the inclusion of magnification bias and extended source structure does not substantially enhance the probability of this faint central image to have magnifications above unity.

In the case of high dynamic range maps, however, central images with $\mu \ll 1$ can still be detected. In such cases equation (28) is no longer valid and we have to find a new estimate for the probability. To do this, we insert equation (25) into the simplified lens equation, equation (14), and arrive at

$$r_s = \frac{1}{2} r_{\rm caust,1}\left[\left(1-\frac{\mu_c}{\mu}\right)^{-1/4} + \left(1-\frac{\mu_c}{\mu}\right)^{+1/4}\right]. \tag{29}$$

For $\mu \to \infty$, the source position goes to $r_{\rm caust,1}$, as expected. In the case $\mu = \mu_4 = -10^{-3}$ (the magnification is negative because the parity of the central image created by the BH is -1), the source position $r_s \approx 1.15\, r_{\rm caust,1}$, assuming $r_c = 0.05$ and $m = 0.002$. The probability of being able to observe this image is then $\approx 2\pi r_{\rm caust,1}(r_s - r_{\rm caust,1})/(\pi r_{\rm caust,2}^2)$, which is ~ 8 per cent for the above given values of r_c and m. If $r_c \sim 0.05$, the currently known sample of 20–30 radio gravitational lens systems – most of which have a typical dynamic range of the order of few times 10^2 up to possibly 10^3 in the brightest cases (e.g. PKS 1830–211, B0218+357) – could therefore contain several systems with central images that are observable once the dynamic range in radio observations of these systems can be improved by an additional factor of 5–10. To separate the two central images, which are only a few milliarcseconds apart, one obviously requires high-resolution very long baseline interferometry (VLBI) observations.

2.2 Elliptical isothermal density distribution with black holes

The spherical case we studied in the previous subsection is idealized, since galaxies nearly always show some ellipticity. In this section, we will study the critical curves and caustics for a more realistic elliptical density distribution plus a black hole. The critical curves can be found by solving equation (5) numerically and the caustics are found using the lens mapping (equation 3). Fig. 3 shows the critical curves and caustics structure as a function of black hole mass for an elliptical density mass distribution with $q = 0.7$ and again $r_c = 0.05$. When there is no black hole at the centre (Fig. 3a), one sees the well-known critical curves and caustics. When a source is inside the diamond caustic, there are five images. When a source is outside the diamond but inside the elliptical caustic, there are three images. When the source moves further outside, there is only one single image. The image configurations for three source positions are illustrated in the same panel. Usually, the central images are quite faint and difficult to observe. Now as we include a black hole mass with $m = 0.002$ (cf. equation 7), an additional small critical curve appears very close to the centre (too small to be seen), and this maps to the middle elliptical caustic. A source outside the diamond but inside this middle elliptical caustic has two images. This is analogous to Fig. 1(b). When a source moves from infinity to the origin, the image number changes according to $2 \to 4 \to 2 \to 4$, with each caustic crossing either increases or decreases the number of images by two. When the black hole mass is further increased to $m = 0.01$ (Fig. 3c) the innermost critical curve becomes larger while the middle critical curve shrinks – their two corresponding caustics also approach each other. When the black hole mass is increased further to or above a critical value, ≈ 0.02 (a value slightly larger than that in the spherical case), the two inner critical curves and their corresponding caustics cancel each other, and one is left with an elliptical critical curve and a diamond caustic at the centre (an example is shown for $m = 0.03$); this caustic separates the outer two image regions from the inner four image regions. In either region, the central images have been suppressed by the black hole. The behaviour in the elliptical density distribution case is qualitatively similar to the spherical case, the main difference is that the ellipticity breaks the spherical symmetry and changes the central degenerate caustic point in the spherical case into the central diamond (compare Figs 1 and 3); the caustic change owing to ellipticity is similar to the case without central black holes (see, e.g., Schneider et al. 1992).

3 DISCUSSION

As clearly demonstrated in Figs 1–3, central black holes in gravitational lenses introduces qualitatively new features in the critical curves and caustics. For realistic black hole masses, the black hole introduces a new region in the source plane that has four images. However, this additional four-image region does not

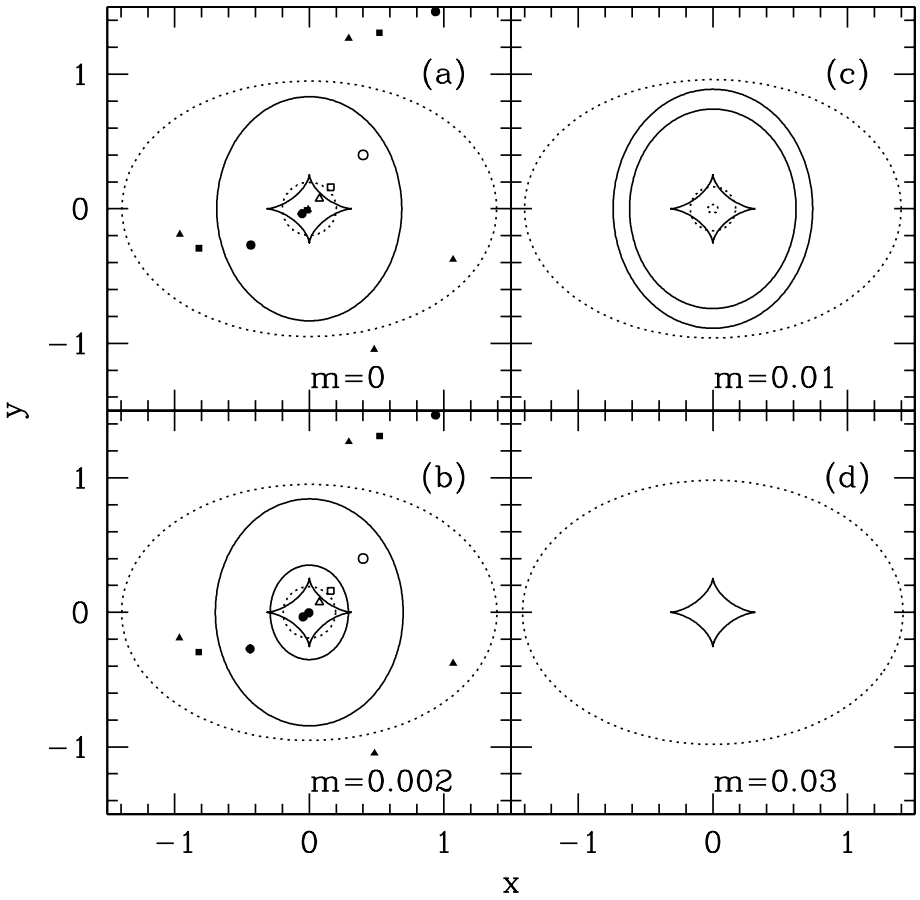

Figure 3. The critical curves (dotted) and caustics (solid) for an isothermal ellipsoid plus a black hole. The core radius is taken to be $r_c = 0.05$ and the axial ratio is 0.7. All the lengths are in units of the critical radius (equation 2), and the dimensionless black hole mass (m) is given in units of equation (4). For the two left-hand panels the images are shown for three source positions, indicated by an open triangle, square and circle; their corresponding image positions are shown as filled triangles, squares and circles. For (a), a source outside the solid ellipse will have one image, and then three images as the source crosses the elliptical caustic and five images when the source crosses the diamond caustic. For bottom left-hand panel, as a source moves from infinity to the centre, the number of images changes according to $2 \rightarrow 4 \rightarrow 2 \rightarrow 4$, with each caustic crossing changing the number of images by 2.

help to resolve the problem of the apparent excess of quadruple lenses relative to double lenses (King & Browne 1996; Kochanek 1996b). The reason is that these four-image configurations have two very faint images at the centre and two bright images outside, which are very different from the observed quadruple lenses where the images are roughly on a circle from the lens centre. The image closest to the black hole is the faintest image; for the case shown in Fig. 3(b), this image is about a factor of 10^{-5} times fainter than the brightest one. As shown in Section 2.1.1, there is only a negligible probability that the central images can reach magnifications of the order of unity. However, we find that there is a non-negligible probability ($\sim$8 per cent for $r_c = 0.05$ and $m = 0.002$) that the central image can reach magnification $\gtrsim 10^{-3}$, with the two distinct central images separated by about $10^{-3}b$ ($\sim$milli-arcseconds). Such images can in principle be detected with future high dynamic range and high-resolution VLBI observations. Note that this probability obviously depends on the values of m and r_c, and is uncertain since for the latter only upper limits are available at present.

The massive black holes also complicate the interpretation of core radius inferred because of the lack of central images. The central image will be completely suppressed for all source positions if the black hole mass exceeds the critical value as given in equation (13). This critical mass is reached when the ratio of the mass of the black hole to the galaxy mass in the inner parts [more precisely, M_0 in equation (4)] is approximately equal to the core radius in units of the critical angle b. For a galaxy with velocity dispersion of 250 km s^{-1}, the mass of the central black hole is $\sim 4 \times 10^8\,\mathrm{M}_\odot$, and $M_0 \sim 1.6 \times 10^{11}\,h^{-1}\,\mathrm{M}_\odot$. The black hole is super-critical when $r_c \lesssim 0.002$; in physical units, this implies an upper limit on the core radius of about $\sim$10 pc for typical lens configuration with $R_{cr} \sim$ few kpc. This upper limit is usually not reached except for lens systems with a favourable image geometry such as B1030+074 (Norbury et al., in preparation). However, the presence of central black holes can also suppress the central image even when it is much below the critical value in some regions (see Figs 1b and 3b). The zone of influence of the black hole is characterized by the $r_{caust,1}$ (equation 16) in the spherical case: when the source is inside the zone [$r_s < r_{caust,1} \approx (2m/r_c)^{1/2}$], the central image is destroyed. For a given source position r_s, the central image disappears when the black hole mass satisfies

$$m \gtrsim \frac{r_c r_s^2}{2} \approx \frac{r_c}{2(\mu_1 - 1)^2}, \tag{30}$$

where in the last step we have replaced the source position on the right-hand side by the magnification of the brightest image μ_1

using equation (20). For a galaxy with $\sigma = 250\,\mathrm{km\,s^{-1}}$, $m \approx 0.002$ and $\mu_1 \sim 4$, the central image will be destroyed when $r_c < 0.04$ ($\sim$100 pc for a typical critical radius of a few kpc). More generally, the influence of black holes on the core radius constraint has to be obtained from detailed modelling. Equation (30) also highlights that the best lenses to search for central images are systems with low magnifications. In such systems, the source is closer to the outer caustic ($r_{\mathrm{caust},2}$) and hence is more likely to be outside the zone of influence. As a result, the central images are less likely to be suppressed by the black hole. Unfortunately, these systems also have large flux ratios between the two bright out images (cf. equations 20 and 21). Since lens surveys favour systems with large magnifications owing to magnification bias and systems with small flux ratio, it is not surprising that very few lenses discovered so far show central images, perhaps as a result of both small core radii and central black holes in gravitational lenses.

In this paper, we have only considered the lensing effects of central black holes embedded in isothermal spheres. While the assumption of isothermality appears plausible (see Section 2), recent numerical simulations seem to suggest that the dark matter volume density may scale as $\rho(r) \propto r^{-\gamma}$ with $\gamma \sim 1$–1.5 in the inner region (e.g. Navarro, Frenk & White 1997; Moore et al. 1998), which is somewhat shallower than the isothermal profile, $\rho(r) \propto r^{-2}$. Furthermore, *Hubble Space Telescope* (*HST*) observations indicate that the inner light profiles are correlated with the luminosity and hence with the black hole mass (Faber et al. 1997). A realistic analysis should also account for the coupling between dark matter and baryonic (light) components. These issues are not considered here, but it would be very interesting to perform a more detailed analysis when the observational data improve further.

ACKNOWLEDGMENTS

We thank Ian Browne for helpful discussions and Chuck Keeton for insightful criticisms on a draft of the paper. HJW thanks the visitor programme of Jordell Bank Observatory for financial support.

REFERENCES

Burke W. L., 1981, ApJ, 244, L1
Fabbiano G., 1989, ARA&A, 27, 87
Faber S. M. et al., 1997, AJ, 114, 1771
Ferrarese L., Merritt D., 2000, ApJ, 539, L9
Gebhardt K. et al., 2000, ApJ, 539, L13
Grogin N. A., Narayan R., 1996a, ApJ, 464, 92; 1996b, ApJ, 473, 570 (erratum)
Hinshaw G., Krauss L. M., 1987, ApJ, 320, 468
Ibata R. A., Lewis G. F., Irwin M. J., Lehar J., Totten E. J., 2000, AJ, 118, 1922
Jackson N., Helbig P., Browne I., Fassnacht C. D., Koopmans L., Marlow D., Wilkinson P. N., 1998, A&A, 334, L33
Kassiola A., Kovner I., 1993, ApJ, 417, 450
Kauffmann G., Haehnelt M., 2000, MNRAS, 311, 576
Keeton C. R., Kochanek C. S., 1998, ApJ, 495, 157
Keeton C. R., Kochanek C. S., Seljak U., 1997, ApJ, 482, 604
King L., Browne I. W. A., 1996, MNRAS, 282, 67
Kochanek C. S., 1995, ApJ, 445, 559
Kochanek C. S., 1996a, ApJ, 466, 638
Kochanek C. S., 1996b, ApJ, 473, 595
Kormann R., Schneider P., Bartelmann M., 1994, A&A, 284, 285
Kormendy J., Richstone D., 1995, ARAA, 33, 581
Magorrian J. et al., 1998, AJ, 115, 2285
Maoz D., Rix H.-W., 1993, ApJ, 416, 425
Moore B., Governato F., Quinn T., Stadel J., Lake G., 1998, ApJ, 499, L5
Narayan R., Blandford R., Nityananda R., 1984, Nat, 310, 112
Navarro J. F., Frenk C. S., White S. D. M., 1997, ApJ, 490, 493
Rix H.-W., de Zeeuw P. T., Carollo C. M., Cretton N., van der Marel R. P., 1997, ApJ, 488, 702
Silk J., Rees M. J., 1998, A&A, 331, L1
Schneider P., Ehlers J., Falco E. E., 1992, Gravitational Lenses. Springer-Verlag, New York
Wallington S., Narayan R., 1993, ApJ, 403, 517
Witt H. J., Mao S., 1995, ApJ, 447, L105

This paper has been typeset from a TEX/LATEX file prepared by the author.